



ORIGINAL ARTICLE

Preparation and evaluation of poplar waste derived adsorbent for dye removal



Xiaojing Qin^a, Xiangwang Zeng^b, Song Cheng^{b,c,d,*}, Baolin Xing^{b,c,d},
Dengke Jiang^e, Saidan Zhao^b, Changliang Shi^{b,c}, Zhiguo Zhang^{b,c}, Qiang Wang^{b,c},
Chuanxiang Zhang^{b,c}

^a School of Surveying and Land Information Engineering, Henan Polytechnic University, Jiaozuo 454003, China

^b College of Chemistry and Chemical Engineering, Henan Polytechnic University, Jiaozuo 454003, China

^c Collaborative Innovation Center of Coal Work Safety and Clean High Efficiency Utilization, Jiaozuo 454003, China

^d Henan International Joint Laboratory of Clean Coal Utilization, Henan Polytechnic University, Jiaozuo 454003, China

^e Chifeng Shanjin Silver and Lead CO.,LTD, Chifeng, Inner Mongolia, 025450, China

Received 11 January 2023; accepted 10 April 2023

Available online 18 April 2023

KEYWORDS

Poplar waste;
Dye wastewater;
Adsorption mechanism;
H₂ rich fuel gas;
Methylene blue

Abstract Poplar waste is employed to prepare the high quality adsorbent (PWA) using one-pot method for methylene blue (MB) removal from wastewater. The H₂ rich fuel gas is recycled during preparation process. The adsorption isotherms and adsorption kinetics are used to describe the MB adsorption process. The MB adsorption capacity of the PWA is 254.21 mg/g based on the Langmuir model calculation. Pseudo-second-order model describe well with the adsorption kinetic process. The MB column adsorption process of the PWA is analyzed by the Thomas and Yoon-Nelson, which indicates that the adsorption capacity is 54 mg/g and saturation time is 540 min. PWA has excellent reusability, which still maintains 75.59% MB adsorption amount after five cycles. The MB adsorption mechanism of PWA includes chemical functional groups, electrostatic interaction and pore filling. Density functional theory calculation indicates that hydroxyl groups play an important role in MB adsorption process. MB adsorption performance of PWA is investigated in the actual water with excellent MB removal. This result demonstrates that PWA could be acted as the recoverability and efficient adsorbent for MB removal from wastewater.

© 2023 The Author(s). Published by Elsevier B.V. on behalf of King Saud University. This is an open access article under the CC BY-NC-ND license (<http://creativecommons.org/licenses/by-nc-nd/4.0/>).

1. Introduction

The environment of our world has seriously been polluted owe to rabid industrial, especially water environment (Azha et al., 2021; Wang et al., 2022a). The various of toxic dyes cause the pollution

of water environment, which has attracted wide attentions (Zhang et al., 2020a; Wang et al., 2022b). The textile industry has produced huge amount of dye wastewater, which is the primary source of the dye wastewater due to fact that it is water-consuming industry (Gopalakrishnan et al. 2020; Gao et al. 2021). Besides, many

* Corresponding author at: College of Chemistry and Chemical Engineering, Henan Polytechnic University, Jiaozuo 454003, China.
E-mail address: cskmust@163.com (S. Cheng).

dyes are hazardous, carcinogenic and mutagenic for the aquatic life and human beings, which cannot self-degradation in the aqueous solution due to poorly biodegradable (Uddin et al., 2021; Wang et al., 2020). MB is a kind of water-soluble dyes, which is usually found in wastewater (Toledo et al., 2020). Despite MB presents in a very small amount, it still can irritate the skin and eye by damaging DNA and proteins (Silva et al., 2021). Therefore, it is essential to separate dye from contaminated water using an effective method to eliminate the harm for the environment and human beings.

Adsorption (Zhang et al., 2020b), biological (Li et al., 2021a), electrochemical (Li et al., 2020a), photodegradation (Cheng et al., 2022a) and chemical oxidation (Chang et al., 2009) are the common technologies for dye wastewater removal. Adsorption technology is considered as an efficient method to treat dye wastewater owe to the advantages such as high efficiency, low cost and the recyclability of separating (Xiao et al., 2021). The adsorbent such as activated carbon (Wan et al., 2018), biochar (Pagalan et al., 2020) and molecular sieve (Shabaan et al., 2020) are usually used to treat dye wastewater. In order to realize the economic and environmental friendly of the dye wastewater removal process, the precursors prepared adsorbent should be sustainable and cheap (Wang et al., 2021a,b,c). Biomass waste is kind of waste, which is renewable resources due to the photosynthesis of biomass (Cheng et al., 2022c). Therefore, biomass waste can be used as the promising precursor for preparation of high-efficiency adsorbent to govern dye wastewater.

Pyrolysis is a kind of method to utilize the biomass waste to prepare the biochar for dye wastewater removal. However, the adsorption performance of biochar cannot meet the requirements of the wastewater treatment plant in the actual application process, especially large-scale application. The physical and chemical activation methods are employed to expand the pore structure of biochar for improving its adsorption performance. KOH, K_2CO_3 , H_3PO_4 , $ZnCl_2$, H_2O and CO_2 are common chemical and physical activation agents to prepare high-efficiency adsorbent (Li et al., 2020b; Menya et al., 2018). Danish et al. (2018) have used the wood biomass as raw material to prepare the adsorbent by chemical activation agents such as H_3PO_4 , $ZnCl_2$ and KOH for MB removal from wastewater with high MB adsorption capacity. Several researchers reported that the production process of adsorbent includes two steps (Akhouairi et al., 2019; Suganya et al., 2017; Xiao et al., 2020). The first step is to produce the biochar by pyrolysis of biomass waste (Jawad et al., 2021). The second step is the activation of biochar by chemical and physical activation method to expand its surface area and pore volume (Zhang et al., 2021). However, the production process of adsorbent is time-consuming and energy consumption, resulted in high production cost (Li et al., 2021b). The pyrolysis exhaust is also ignored, which causes the pollution of environment. Therefore, simple and low-cost preparation method of high-efficiency adsorbent is urgent. Besides, the pyrolysis exhaust should be recycled to eliminate the possible pollution for the environment (Cheng et al., 2021b).

Poplar waste is a kind of wood waste, which is produced from poplar planting and processing process. The annual products are very huge. Finding an efficient utilization method of poplar waste is necessary. Therefore, it will be necessary to study the comprehensive utilization of poplar waste, and provide guidance for the similar species. Chen et al. (2023) prepared the magnetic porous carbon adsorbent using the poplar sawdust as feedstock for the tetracycline removal for wastewater with the adsorption capacity of the 288.2 mg/g. Heibati et al. (2015) reported that the activated carbon prepared from poplar woods is used as the economical adsorbents for the rapid removal and fast adsorption of Acid Red 18 dye from the aqueous solution. Aghdasinia et al. (2021) prepared the adsorbent derived from the poplar leaf for adsorption of basic yellow 2 from aqueous solution with the adsorption capacity of the 51.282 mg/g. Therefore, the poplar waste could be used as the feedstock to prepare the adsorbent for wastewater treatment.

In this work, poplar waste is employed to produce the PWA for MB removal from wastewater via a facile one-pot method. The pyrolysis exhaust is recycled during preparation process, which could be used as the fuel gas. The adsorption equilibrium, kinetics and thermodynamic process are systematically employed to analyze MB removal process. Involved adsorption mechanisms are investigated. The adsorption performance of PWA in the fix-bed adsorption is also investigated for the actual application. Density functional theory is used to further analyze the MB adsorption process. MB adsorption on PWA is carried out in the actual wastewater to investigate the actual application of PWA.

2. Materials and method

2.1. Materials

Poplar waste is collection from Yunnan province of China. Potassium carbonate, absolute alcohol and MB are ordered from Sinopharm Chemical Reagent Co. Ltd., China.

2.2. Preparation method

20 g poplar waste is mixed with Na_2CO_3 in the 200 mL distilled water, which is stirred for mixing evenly. And then the drying oven is employed to dry the mixture at 80 °C for 24 h. The dry mixture is placed into tube furnace with heating temperature of 900 °C under anaerobic environment. The N_2 is used as carrier gas in the preparation process. When the temperature reached 900 °C, the steam is injected in the tube furnace with the flow rate of 1.5 mL/min. Finally, the steam is closed and N_2 is injected in tube furnace until room temperature. The pyrolysis exhaust produced from tube furnace is recycled to investigate its gas composition for resource utilization, achieving the no pollution generation during preparation process. The original biochar without K_2CO_3 and steam activation is also prepared to compare the adsorption performance of PWA under same experiment conditions. After cooling, the solid residues are PWA and original biochar in the tube furnace.

2.3. Characterization

Quantachrome Autosorb apparatus is used to investigate the pore structure of sample. The surface properties of sample are analyzed using the X-ray photoelectron spectroscopy (XPS). Scanning electron microscopy (SEM) is used to observe the surface morphologies of sample. Fourier transform infrared spectroscopy (FTIR) is employed to detect the chemical property of sample. The ordered/disordered crystal structures of samples are analyzed by the Ramascope spectroscopy. The Zeta PALS is used to detect the Zeta potential of sample.

2.4. Adsorption experimental

Batch adsorption experiments are conducted in a series of 250 mL volumetric flasks containing different adsorbent dose of adsorbent and 100 mL of MB solution 100–300 mg/L. The volumetric flasks are shaken in a gas bath thermostatic oscillator with shaking speed of 300 rpm/min until the equilibrium reached. After equilibrium is attained, the amount of residual MB concentration is detected using UV–Vis spec-

trophotometer. The amount of MB retained on the adsorbent, q_e (mg/g), is calculated at equilibrium from the following equation:

$$q_e = \frac{V(C_0 - C_e)}{M} \quad (1)$$

where C_0 (mg/L) and C_e (mg/L) are the initial and equilibrium concentration of MB solution, respectively, V is the volume of solution (L), and M is the weight of the adsorbent (g). The adsorption isotherm models are presented in [Table S1](#).

Adsorption kinetic studies are conducted in a series of 250 mL volumetric flasks using methods similar to those described previously. Aqueous samples are collected at different time intervals and the MB residual concentrations are measured using UV-Vis spectrophotometer. The amount of MB adsorbed over time, q_t (mg/g), is obtained by:

$$q_t = (C_0 - C_t)V/M \quad (2)$$

where C_t (mg/L) is the liquid-phase concentration of MB solution at time t (min). The adsorption kinetic models data are presented in [Table S2](#).

2.5. Fixed-bed column

The column adsorption experiment is carried out in the fixed bed system with the MB concentration of 100 mg/L. MB solution is pumped in the fixed bed system using peristaltic pump. The feed flow rate is 5 mL/min in adsorption process. A small amount of suspensions are taken from fixed bed system to detect MB concentration at special time intervals. UV-Vis spectrophotometer is employed to detect the residual MB concentration. The MB adsorption capacity (Q_m , mg/g) is investigated using following equation.

$$Q_m = \frac{VC_0}{M} \int_{t=0}^{t=t_{tot}} \left(1 - \frac{C_t}{C_0}\right) dt \quad (3)$$

Q_m (mg/g) denotes MB column capacity. V is the flow rate (mL/min) and total flow time is denotes as t_{tot} . The time of the C_t/C_0 of 0.95 and 0.05 is saturation time and breakthrough time, respectively. [Table S3](#) lists the column fitting models, which are used to investigate the MB adsorption performance.

3. Results and discussion

3.1. Pore structure and surface morphology analysis

[Fig. 1](#) shows the nitrogen adsorption curve and pore distribution of PWA. As [Fig. 1a](#) shown, PWA has larger Brunauer Emmett Teller (BET) specific area. It can be explained that the C element on PWA is consumed by C- Na_2CO_3 and C- H_2O reactions, which produces a large number of pores. These reactions can generate the activation gases such as CO_2 , H_2 , and CO , which contribute to forming ultramicropores in mesopore walls ([Saygili and Guzel, 2016](#)). Besides, these gases can promote the expansion of pore structure when these gases diffuse to the surface of PWA. [Fig. 1a](#) shows that the nitrogen adsorption curve of PWA has the hysteresis loop, highlighting the presence of mesoporosity. Therefore, PWA has well-developed pore structure, which provides large number of adsorption sites, contributing to MB removal ([Wang et al., 2017](#)). Pore size distribution can affect the adsorption capacity

of adsorbent for different sizes and shapes targeted contaminant, which determines special application of adsorbent. As shown in [Fig. 1b](#), the sharpest peak range from 1 to 5 nm, indicates that a majority of the pores fall into the range of mesopore. As we all known, the adsorption counts on the pore structure besides the surface chemical properties of adsorbent. [Cheng et al. \(2016\)](#) reported that adsorption occurs when the pore diameter of adsorbent is at least 1.7 times larger than that of the adsorbate. The minimum molecular size of MB is about 0.8 nm. The average pore size of the PWA is 2.33 nm. Therefore, it is accessible to adsorb MB.

The micrographs of PWA can be observed by SEM images. [Fig. 1c](#) indicates that the well-developed visible pores are found in the PWA. This result demonstrates that steam combined with K_2CO_3 activation contributes to generating pore in the PWA. These reactions form a large number pores. Besides, the generated gases can act as the ‘‘cleaner’’ to clean the formed pore structure when these gases escape from PWA. [Fig. 1c](#) indicates that PWA has a great number of pores, which is consistent with above analysis. The micrograph and pore structure analysis indicates that PWA can be employed as an efficient adsorbent to remove MB from wastewater.

3.2. XPS and FTIR analyses

[Fig. 2a](#) shows the C 1s spectrum of PWA. As [Fig. 2a](#) shown, the peaks located at 284.51 eV, 285.19 eV, 286.53 eV are corresponded to C-C, C-O and C=O groups, respectively ([Xue et al., 2021](#)). Similarly, the C-O and the C=O bond of O 1s spectrum are appeared at 532.58 and 533.46 eV, respectively ([Luo et al., 2015](#)). These results indicate that oxygen-containing groups such as quinone, carboxyl, hydroxy, and lactone probably generate in PWA, which contribute to MB adsorption. [Xue et al. \(2021\)](#) point out that oxygen-containing group of adsorbent is conducive to organic dye removal. FTIR analyses of PWA are shown in [Fig. 2c](#). As shown in [Fig. 2c](#), O-H stretching vibration is appeared at 3412 cm^{-1} and C=O group is found at 1578 cm^{-1} ([Cheng et al. 2022b](#)). PWA has the peak at 1166 cm^{-1} , which is C-O group. The C-H (benzene derivatives) group appears at peak of 490 cm^{-1} ([Wang et al. 2023](#)). FTIR analyses are consistent with XPS results.

3.3. Raman analysis

Raman spectra of PWA and original biochar are used to analyze the activation process of the PWA. The characteristic D band and G band appear at around 1350 and 1600 cm^{-1} , corresponding to the disordered (Csp3) and graphitic (Csp2) carbon structures, respectively ([Fig. 3](#)). The I_D/I_G ratio of PWA (0.72) is large compared to the original biochar (0.63). The result demonstrates that etching of Csp2 by Na_2CO_3 and H_2O is lower than Csp3, indicating formation of new functional groups in PWA ([Kazak et al., 2017](#)). It also indicates that the activation process promotes the formation of disordered structure in PWA ([Rakesh et al., 2015](#)).

3.4. Adsorption isotherms studies

The MB adsorption capabilities of PWA and original biochar are shown in [Fig. 4a](#) to compare their adsorption performance

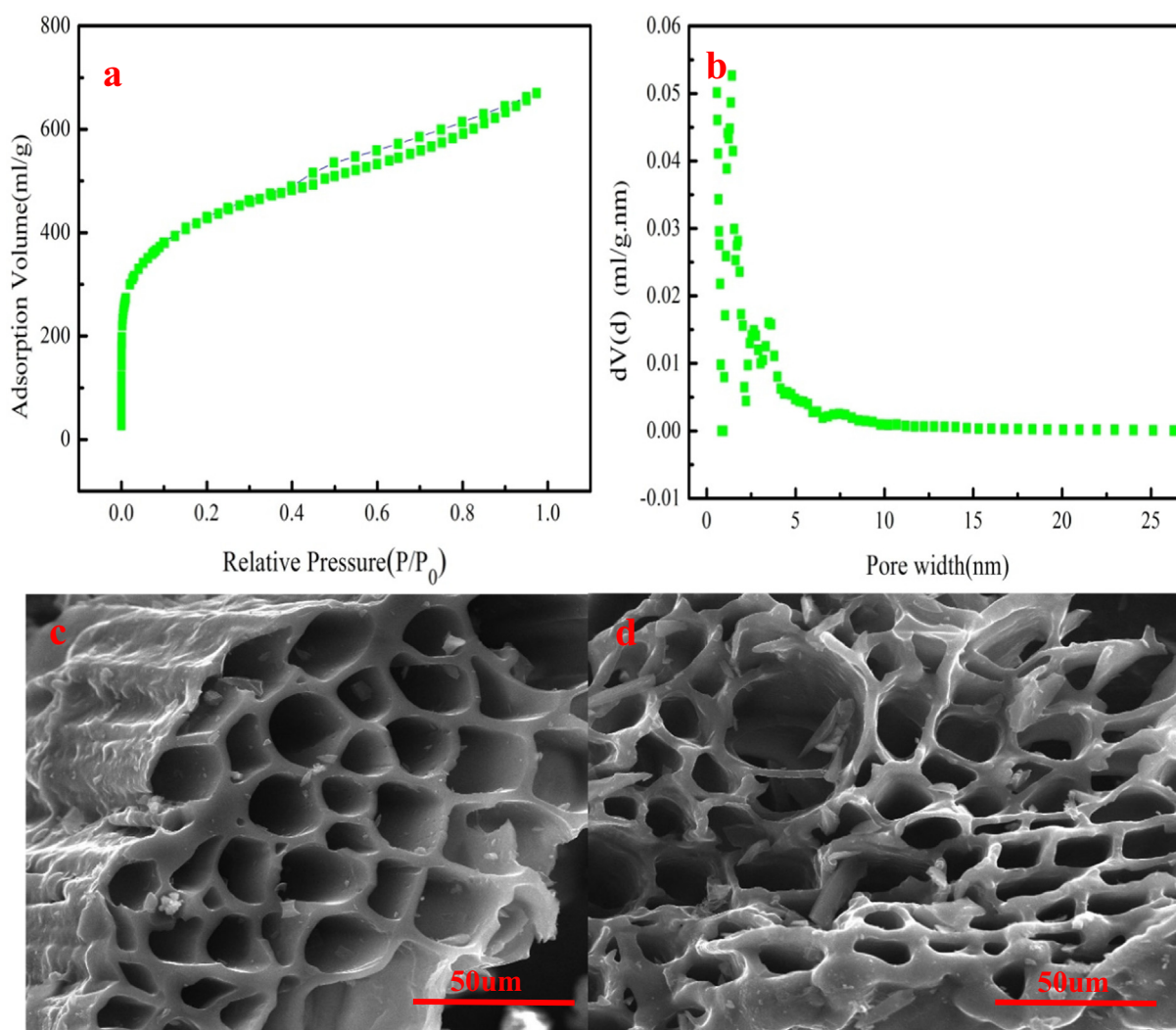


Fig. 1 The N_2 adsorption isotherm and pore size distribution of PWA (a–b), SEM micrographs of PWA (c–d).

at different concentrations. As Fig. 4a shown, MB adsorption capability of PWA is larger than that of original biochar at different concentrations. It indicates that the preparation method of PWA is feasible. MB adsorption behavior on PWA is analyzed by four kinds of adsorption isotherms. Table 1 lists the fitting results, which are obtained from MB adsorption data fitting these models. As Table 1 shown, Langmuir isotherm can describe MB adsorption behavior on PWA with large R^2 value. It also indicates that MB adsorption performance on PWA can be more exactly predicted by Langmuir isotherm model. MB adsorption on PWA is monolayer adsorption based on the report of the Xia et al. (2021). MB adsorption amount of PWA generally increases as adsorption temperature increases (Table 1). This phenomenon demonstrates that high adsorption temperature is conducive to MB adsorption in the actual application process. This result also demonstrates that MB adsorption performance is endothermic nature (Chowdhury et al., 2020). This phenomenon can be explained that the surface activity and kinetic energy of PWA increase with increasing in adsorption temperature (Amran and Zaini, 2021). Interaction forces between solute and adsorbent is larger than that of the solute and solvent, resulted in large MB

adsorption capability at high adsorption temperature. Fig. 4b shows MB adsorption data fitting Langmuir model.

The feasibility of MB adsorption on PWA is investigated by the dimensionless factor R_L . The R_L can be calculated by the following equation.

$$R_L = \frac{1}{1 + KLC_0} \quad (4)$$

MB adsorption process is feasible with $R_L < 1$. R_L values (0.0015–0.00650). This result demonstrates that MB adsorption on PWA is feasible.

MB adsorption amount of others similar adsorbents are listed in Table 2 to compare with PWA. Table 2 indicates that PWA has larger MB adsorption capability than that reported adsorbents. Therefore, PWA is the promising adsorbent for MB removal.

3.5. Adsorption kinetics studies

MB adsorption kinetics process is described by four kinds of the adsorption kinetics models. The fitting results of MB adsorption on PWA using adsorption kinetics models are sum-

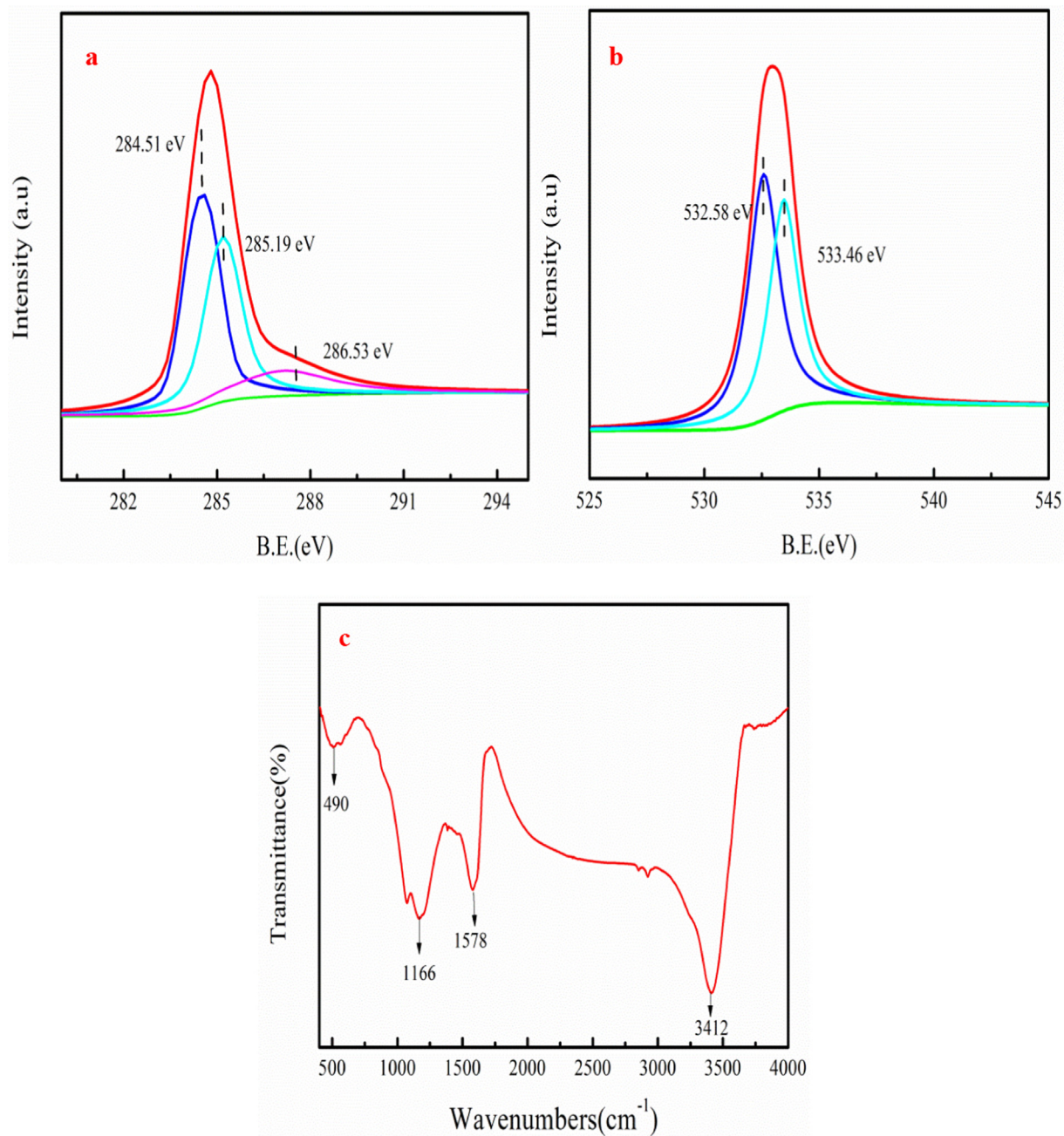


Fig. 2 FTIR spectra of PWA (a), C 1s spectrum (b) and O 1s spectrum (c) of XPS survey spectrum.

marized in Table 3. As Table 3 shown, MB adsorption kinetics process can be more exactly analyzed by the pseudo-second order model because of large R^2 value among adsorption kinetics models at different MB concentrations. Therefore, pseudo-second order model is employed to predict MB adsorption kinetic process. This result demonstrates that the adsorption site of PWA mainly determines MB adsorption rate (Lacerda et al., 2015). As Table 3 shown, rate constant K_2 of pseudo-second order kinetic model decreases as MB concentration increases. Wang et al. (2021a,b,c) pointed out that the increasing of dye concentration increases the competition between adsorption site and dye molecule. Therefore, the

adsorption rate of high MB concentration of PWA is low compared to low MB concentration. The fitting results using pseudo-second order model are shown in Fig. 5 at different MB concentrations. Besides, the rate-limiting step of MB adsorption on PWA is investigated by the Intraparticle diffusion model. Table 3 indicates that the C values increase as MB concentration increases, indicating that MB adsorption resistance is large at high MB concentration. The C values are range from 99.09 to 243.99, which are large than zero. This phenomenon indicates that Intraparticle diffusion isn't the rate-limiting step for MB adsorption on PWA (Cheng et al. 2021a).

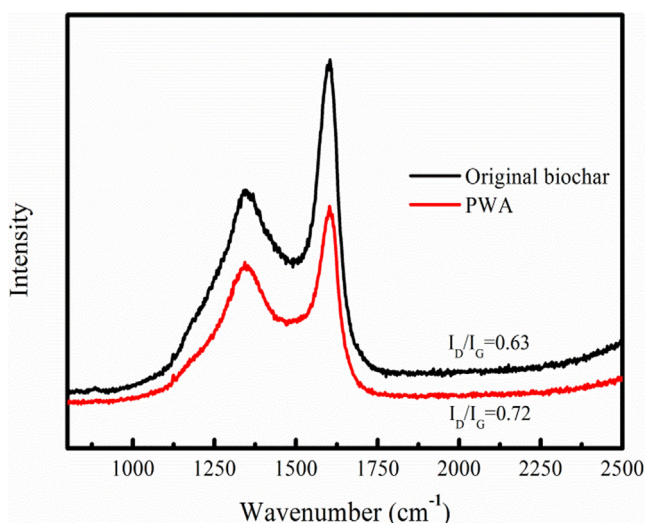


Fig. 3 Raman spectra of original biochar and PWA.

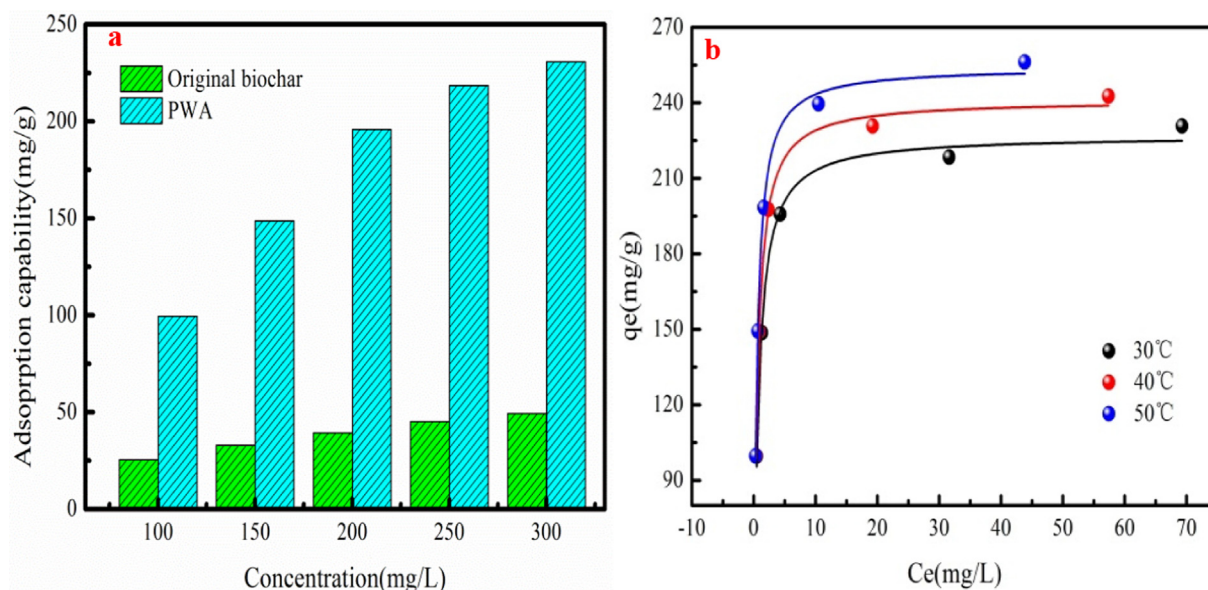


Fig. 4 MB adsorption performance of original biochar and PWA at different concentrations (a) and MB adsorption data fitting the Langmuir isotherm model (b).

3.6. Adsorption thermodynamics studies

As Table 1 shown, adsorption temperature has positive influenced on MB adsorption. MB adsorption amount increases from 226.98 mg/g to 254.21 mg/g as adsorption temperature increases from 30 to 50 °C. The reason is that MB kinetic energy increases as adsorption temperature increases. Wang et al. (2017) reported that large kinetic energy is conducive to MB intraparticle diffusion. Therefore, increasing adsorption temperature is conducive to MB adsorption, resulted in large MB adsorption amount at high adsorption temperature.

The thermodynamics parameters such as entropy ΔS , enthalpy ΔH and free energy ΔG are calculated by the following equations.

$$\ln Kd = \frac{\Delta S}{R} - \frac{\Delta H}{RT} \quad (5)$$

$$\Delta G = -RT \ln(Kd) \quad (6)$$

Table 1 The fitting parameters of adsorption isotherm model.

Isotherms	Parameters	Temperature (°C)		
		30	40	50
Langmuir	Q_0 (mg/g)	226.98	241.09	254.21
	K_L (L/mg)	1.54	1.89	2.24
	R^2	0.99	0.99	0.99
Freundlich	$1/n$	0.1524	0.1585	0.1715
	K_F ((mg/g).(L/mg) ^{1/n})	131.26	141.47	150.98
	R^2	0.91	0.87	0.98
Dubinin-Radushkevich	α (mg g ⁻¹)	208.57	222.09	232.58
	β (mol ² J ⁻²)10 ⁻⁸	9.45	7.16	5.32
	R^2	0.90	0.93	0.94
Temkin	R^2	0.89	0.87	0.92

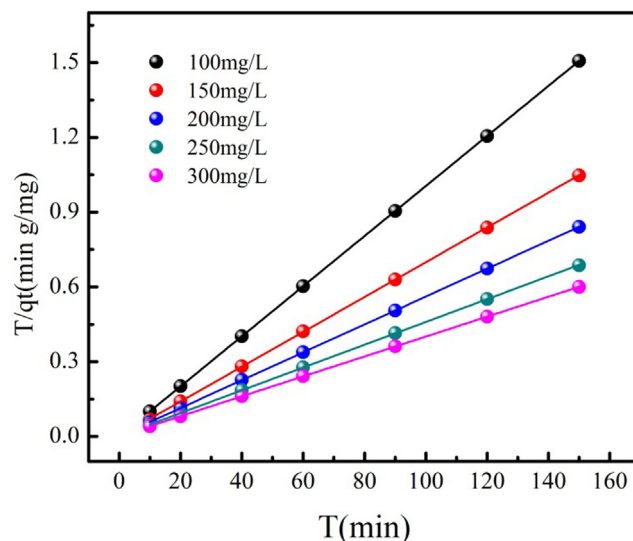
Table 2 Comparison of maximum adsorption capacities, q_m (mg/g) of MB on various adsorbents.

Adsorbent	q_m (mg/g)	Reference
Wood biomass activated carbons	159.8	Danish et al., 2018
Waste seeds aleurites moluccana	178	Postai et al., 2016
Walnut shell-based activated carbon	115.78	Li et al., 2020a
Carbon-doped boron nitride	119.38	Wang et al., 2021b
Activated sugar-based carbon	195.2	Jawad et al., 2021
Karanj fruit hulls activated carbon	239.4	Islam et al., 2017
Bamboo chip activated carbon	305.3	Jawad and Abdulhameed, 2020
Wood activated carbon	59.92	Danish et al., 2018
PWA	254.21	This work

$$K_d = \frac{q_e}{C_e} \quad (7)$$

The slope and intercept of $\ln(K_d)$ vs. $1/T$ plot is shown in Fig. S1. The value of ΔG (-11.89 , -13.39 and -14.62 kJ/mol) indicates that MB adsorption on PWA is spontaneousness owe to negative ΔG value. The ΔG value decreases as adsorption temperature increases. This phenomenon demonstrates that adsorption temperature contributes to MB adsorption on PWA. This result is useful in the actual application process.

Besides, this analysis result is in good agreement with the adsorption isotherms study. The ΔH value is 29.43 kJ/mol, indicating that MB adsorption process is endothermic. The positive value of ΔS (136.52 J/mol) indicates an increase in randomness at the solid/solution interface during adsorption. These results also suggest that some structural changes occur in the adsorbates and adsorbents (Paredes-Laverde et al., 2021).

**Fig. 5** MB adsorption data fitting the pseudo-second order model.**Table 3** The fitting parameters of adsorption kinetic models.

C_0 (mg/L)	qe.cal (mg/L)	K_1 (1/min)	R^2
100	99.45	0.5773	0.92
150	148.50	0.6196	0.94
200	177.34	0.4022	0.88
250	216.32	0.3797	0.90
300	248.31	0.4487	0.86
Pseudo-first-order model			
C_0 (mg/L)	qe.cal (mg/L)	K_2 (g/mg min)	R^2
100	99.60	0.1803	1
150	143.27	0.0494	0.99
200	178.89	0.0134	1
250	218.82	0.0099	0.99
300	250.63	0.0078	0.99
Pseudo-second-order model			
C_0 (mg/L)	C (mg/g)	K_3 (mg/gmin ^{1/2})	R^2
100	99.09	0.0393	0.84
150	148.07	0.0501	0.97
200	173.33	0.4559	0.93
250	210.26	0.0687	0.94
300	243.99	0.5037	0.99
Intraparticle diffusion model			
C_0 (mg/L)	1/a (mg/g)	1/b (mg/g)	R^2
100	98.86	0.1408	0.95
150	147.78	0.1700	0.97
200	170.66	1.5890	0.98
250	206.29	2.3814	0.98
300	241.28	2.6951	0.97
Elovich kinetic models			

3.7. Fixed-bed adsorption

The column adsorption experiment is employed to continuously treat large volume of wastewater containing contaminants using a certain amount of adsorbent, which is useful in the actual application. Fig. 6 shows the breakthrough curve of MB adsorption process. The fitting results are summarized in Table 4. As Table 4 shown, the MB breakthrough time and saturation time are 110 min and 540 min, respectively. While the Q_m of MB adsorption on PWA is 53 mg/g. The column adsorption experiment provides the useful information of MB adsorption performance in the column. These results can further guide the design of Fixed-bed adsorption system in the future. The breakthrough curves obtained from the experimental data fitting the Thomas and Yoon-Nelson models have large R^2 (Table 4). As Table 4 shown, the fitting results of the Thomas mode indicate that MB column adsorption amount and adsorption rate are 28.19 mg/g and 00020 mL min⁻¹ mg⁻¹, respectively. The MB column adsorption amount is lower than that of the adsorption amount calculated from batch adsorption.

The above results demonstrate that PWA can be used in the actual wastewater treatment.

3.8. Adsorption mechanism

The contaminant adsorption mechanism of PWA is useful for the actual application, which can also guide the preparation process of adsorbent. As Fig. 2a shown, the peaks located at 284.51 eV, 285.19 eV, 286.53 eV are corresponded to C—C, C—O and C=O groups, respectively. As Fig. 7a shown, peak positions, peak areas and binding energies of C—C, C—O and C=O groups have slight changed after MB adsorption. The C—O peak area decreases by 9.09% after MB adsorption. While C=O peak area decreases by 4.81% compared to original PWA. The C 1s spectra analyses indicate that the C—O and C=O groups in the phenolic hydroxyl and carboxylic bind with MB sites and involve in MB removal. This result is consistent with the report of the Wang et al. (2017), who pointed out that phenolic hydroxyl and carboxylic in bicchar contribute to dye removal from wastewater. As Fig. 7b shown,

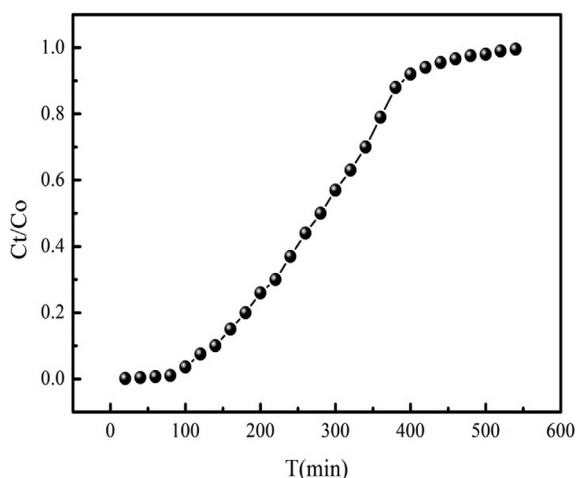


Fig. 6 Breakthrough curve of MB adsorption on PWA.

Table 4 Parameters and coefficients of determination obtained for Thomas and Yoon-Nelson models.

Models	Parameters	MB
Thomas	Q_m (mg g ⁻¹)	54
	Breakthrough time (min)	110
	Saturation time (min)	540
	q_{th} (mg g ⁻¹)	28.19
Yoon-Nelson	K_{Th} (mL min ⁻¹ mg ⁻¹)	0.00020
	R^2	0.9720
	$T_{0.5\%}$ (min)	281.99
Yoon-Nelson	K_{YN} (min ⁻¹)	0.020
	R^2	0.9720

Zeta analysis indicates that surface potential of PWA is negative at around pH = 7. Therefore, electrostatic adsorption between MB and PWA occurs due to the positive of MB surface, which is conducive to MB removal. Fig. 7c shows the FTIR spectra of PWA before and after MB adsorption. Fig. 7c indicates that C=O peak is found in PWA at around 1578 cm⁻¹. However, the C=O peak is shifted to 1594 cm⁻¹ and peak intensity is weakened after MB adsorption. The C—O peak is appeared at 1166 cm⁻¹ in PWA. Compared with PWA, the peak position and peak intensity of C—O are changed after MB adsorption. This result indicates that oxygen-containing functional groups (C=O and C—O) participate in MB adsorption. Besides, PWA with well-developed porous structure provides tremendous pores filling sites for MB adsorption. Possible MB adsorption mechanism of PWA includes chemical functional groups, electrostatic attraction and pore filling. Fig. 7d presents the schematic diagram of possible MB adsorption mechanism.

3.9. Density functional theory calculation

Adsorption mechanism analysis indicates that carboxyl and hydroxyl groups involve in MB adsorption. Density functional theory (DFT) is used to investigate MB adsorption on PWA to decide which one (carboxyl and hydroxyl groups) has more important role in MB adsorption process. PWA has carboxyl and hydroxyl groups. Therefore, simpler biochar-like molecules with carboxyl and hydroxyl groups such as phthalic acid or catechol could be acted as the model biochar. MB adsorption on biochar is investigated by DFT. The binding energies of catechol or phthalic acid interactions with MB are calculated by DFT. The calculated result is shown in Fig. 8. This result shows that it is existence of energy barrier in the MB adsorption process. The binding energy of catechol interactions with MB (−111.09 kJ·mol⁻¹) is smaller than phthalic acid (−49.51 kJ·mol⁻¹), indicating that catechol is easy to bond with MB. The analysis result shows that MB is easier to bind with hydroxyl groups than that of carboxyl groups.

3.10. Reusability

The reusability is used to assess the practicality and economy of adsorbent. Besides, the possible environmental pollution would be avoided by recycling adsorbent from solution after

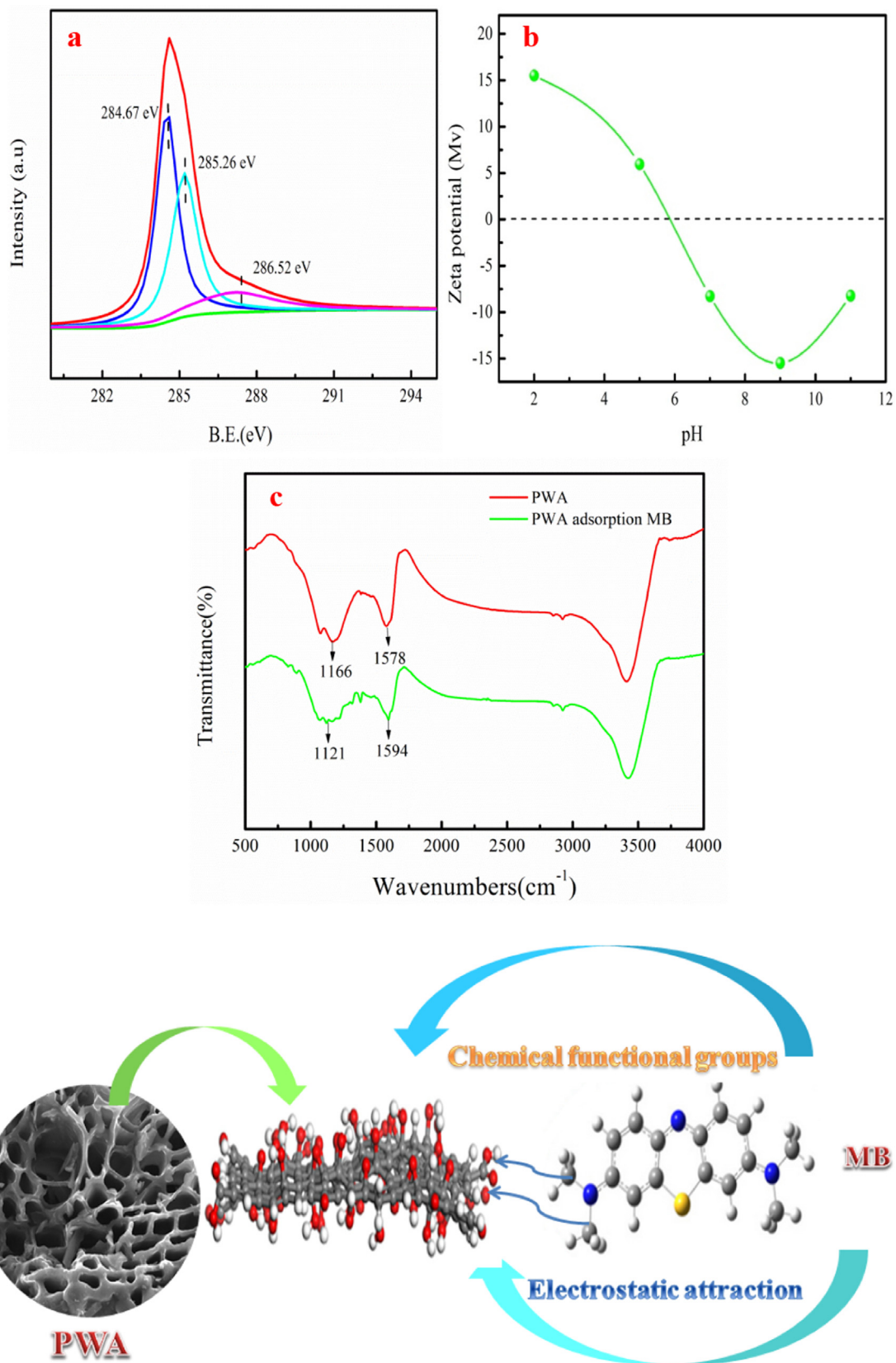


Fig. 7 C 1s spectrum of PWA after adsorption (a), Zeta potential of PWA (b), FTIR spectra of PWA before and after adsorption MB (c) and possible mechanism of MB removal by PWA (d).

use. Therefore, the reusability of PWA is an important parameter, which is investigated by a series of adsorption–desorption experiments. Fig. S2 shows the reusability results of PWA. As shown in Fig. S2, the regeneration cycle of PWA has influenced on MB removal. The MB removal of PWA is 75.59% of the initial level after five cycles. The reason may be that MB molecule in the PWA cannot be removed using desorption agent. Besides, PWA has lost some efficient adsorption sites in the adsorption–desorption experiment.

3.11. Actual wastewater application

The Dianchi Lake water mixed with MB is employed as the actual wastewater to investigate the practical adsorption performance of PWA. The distilled water mixed with MB is used

to compare with the Dianchi Lake water. Fig. S3 shows the MB adsorption performance in the distilled water and dianchi Lake water at MB concentration of 100–200 mg/L. As Fig. S3 shown, the MB removal of PWA in the distilled water is large compared to Dianchi Lake water. It can be explained that impurity ions of Dianchi Lake water have influenced the MB adsorption performance of PWA. In other word, there is existence of competitive adsorption between impurity ions and MB during adsorption process.

3.12. Hydrogen-rich gas recovery

The activation gas in the PWA preparation process is steam, which will produce H₂, CO and other combustible gases. The pyrolysis exhaust is usually discharged into atmosphere,

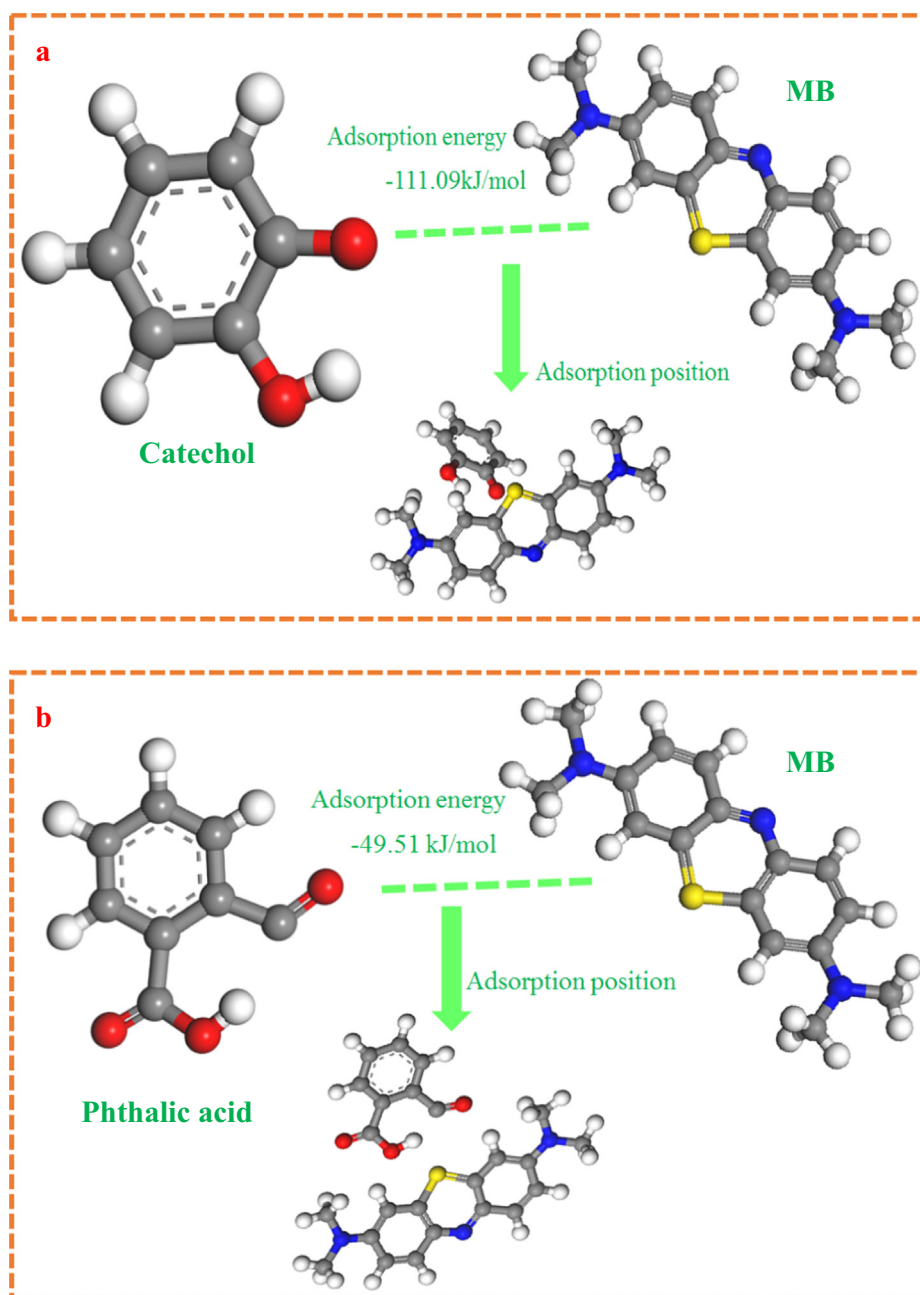
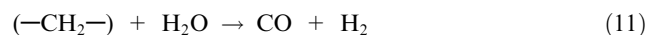
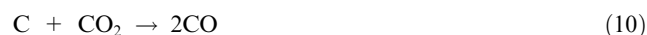
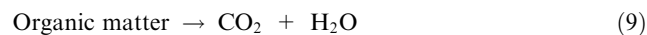


Fig. 8 DFT calculated result of MB adsorption with the hydroxyl (a) and carboxyl groups (b) of PWA.

resulted in environment pollution and waste of resource. The pyrolysis exhaust can be collected and utilized during preparation process. The main compositions of pyrolysis exhaust are as follows: H₂ of 39.61%, CO of 44.39%, CO₂ of 11.05%, CH₄ of 4.37%, C₂H₄ of 0.46% and C₂H₆ of 0.13%. The lower heating value (LHV) of pyrolysis exhaust is 11.82 MJ/m³ according to the calculated method reported by Cheng et al. (2019).

The main components of pyrolysis exhaust are H₂ and CO. The generation of H₂ and CO can be explained by the following equations.



The H₂ and CO are mainly produced by Eq. (8). The byproduct gases have large content of H₂, CO and LHV value, which could be used as the gas fuel for industrial application.

4. Conclusion

PWA has excellent MB adsorption amount with well-developed pore structure, which is successfully prepared using one-pot method. The pyrolysis exhaust is recycled and investigated. The Langmuir and pseudo-second-order kinetic models are employed to investigate MB adsorption process. Thermodynamic study indicates that MB adsorption on PWA is spontaneous and endothermic process. The column adsorption experiments indicate that PWA has efficient adsorption performance in the dynamic adsorption process. The possible MB adsorption mechanisms are surface chemical functional groups, electrostatic interaction and pore filling. Pyrolysis exhaust has high content of the H₂ and large LHV.

CRedit authorship contribution statement

Xiaojing Qin: Conceptualization, Methodology, Writing – original draft. **Xiangwang Zeng:** Conceptualization, Methodology, Writing – original draft. **Song Cheng:** Validation, Supervision. **Baolin Xing:** Validation, Supervision. **Dengke Jiang:** . **Saidan Zhao:** . **Changliang Shi:** . **Zhiguo Zhang:** Investigation. **Qiang Wang:** Investigation. **Chuanxiang Zhang:** Investigation.

Declaration of Competing Interest

The authors declare that they have no known competing financial interests or personal relationships that could have appeared to influence the work reported in this paper.

Acknowledgements

The authors would like to express their gratitude to the Key Scientific and Technological Project of Henan Province (222102320405), National Natural Science Foundation of China (51974110, 52074109 and 52274261), Natural Science Foundation of Henan Province(232300420298), the Fundamental Research Funds for the Universities of Henan Province (NSFRF220417) for financial support.

Appendix A. Supplementary material

Supplementary material to this article can be found online at <https://doi.org/10.1016/j.arabjc.2023.104913>.

References

- Aghdasinia, H., Gholizadeh, M., Hosseini, S.S., 2021. Adsorptive removal of basic yellow 2 onto reed stem and poplar leaf: A comprehensive study. *Sustain. Chem. Pharm.* 24, 100546.
- Akhouairi, S., Ouachtak, H., Addi, A.A., Jada, A., Douch, J., 2019. Natural Sawdust as Adsorbent for the Eriochrome Black T Dye Removal from Aqueous Solution. *Water Air Soil Pollut.* 230, 181–189.
- Amran, F., Zaini, M.A.A., 2021. Valorization of Casuarina empty fruit-based activated carbons for dyes removal - Activators, isotherm, kinetics and thermodynamics. *Surf. Interfaces* 25, 101277.
- Azha, S.F., Shamsudin, M.S., Bonilla-Petriciolet, A., Ismail, S., 2021. Kinetics, process design and implementation of zwitterionic adsorbent coating for dipolar dyes removal in wastewater treatment industry. *Environ. Technol. Innov.* 23, 101763.
- Chang, S., Wang, K., Li, H., Wey, M., Chou, J., 2009. Enhancement of Rhodamine B removal by low-cost fly ash sorption with Fenton pre-oxidation. *J. Hazard. Mater.* 172 (2), 1131–1136.
- Chen, A.X., Wang, N., Tian, Z., Wei, X., Lei, C.J., 2023. One-step synthesis of readily recyclable poplar sawdust-based porous carbon for the adsorption of tetracycline. *Ind. Crop. Prod.* 197, 116621.
- Cheng, S., Zhang, L., Xia, H., Peng, J., Shu, J., 2016. Ultrasound and microwave-assisted preparation of Fe-activated carbon as an effective low-cost adsorbent for dyes wastewater treatment. *RSC Adv.* 6, 78936–79746.
- Cheng, S., Hu, W., Srinivasakannan, C., Xia, H., Zhang, L., Peng, J., Zhou, J., Lin, G., Zhang, Q., 2019. Catalytic pyrolysis of the *Eupatorium adenophorum* to prepare photocatalyst-adsorbent composite for dye removal. *J. Clean. Prod.* 222, 710–721.
- Cheng, S., Liu, Y., Xing, B., Qin, X., Zhang, C., 2021a. Lead and cadmium clean removal from wastewater by sustainable biochar derived from poplar saw dust. *J. Clean. Prod.* 314, 128074.
- Cheng, S., Xing, B., Shi, C., Nie, Y., Xia, H., 2021b. Efficient and selective removal of Pb(II) from aqueous solution by modification crofton weed: Experiment and density functional theory calculation. *J. Clean. Prod.* 280, 124407.
- Cheng, S., Zhao, S.D., Xing, B.L., Shi, C.L., Meng, W.B., Zhang, C. X., Zhang, B., 2022a. Facile one-pot green synthesis of magnetic separation photocatalyst-adsorbent and its application. *J. Water Process Eng.* 47, 102802.
- Cheng, S., Meng, M.L., Xing, B.L., Shi, C.L., Nie, Y.H., Xia, D.P., Yi, G.Y., Zhang, C.X., Hongying Xia, H.Y., 2022b. Preparation of valuable pyrolysis products from poplar waste under different temperatures by pyrolysis: Evaluation of pyrolysis products. *Bioresour. Technol.* 364, 128011.
- Cheng, S., Zhao, S.D., Xing, B.L., Liu, Y.Z., Zhang, C.X., Xia, H.Y., 2022c. Preparation of magnetic adsorbent-photocatalyst composite for dye removal by synergistic effect of adsorption and photocatalysis. *J. Clean. Prod.* 348, 131301.
- Chowdhury, M.F., Khandaker, S., Sarker, F., Islam, A., Rahman, M. T., Awual, M.R., 2020. Current treatment technologies and mechanisms for removal of indigo carmine dyes from wastewater: A review. *J. Mol. Liq.* 318, 114061.
- Danish, M., Ahmad, T., Hashim, R., Said, N., Akhtar, M.N., Mohamad-Saleh, J., Sulaiman, O., 2018. Comparison of surface properties of wood biomass activated carbons and their application against rhodamine B and methylene blue dye. *Surf. Interfaces* 11, 1–13.

- Gao, H.J., Wang, S.F., Fang, L.M., Sun, G.A., Chen, X.P., Tang, S. N., Yang, H., 2021. Nanostructured spinel-type $M(M = \text{Mg, Co, Zn})\text{Cr}_2\text{O}_4$ oxides: novel adsorbents for aqueous Congo red removal. *Mater. Today Chem.* 22, 100593.
- Gopalakrishnan, A., Singh, S.P., Badhulika, S., 2020. Reusable, few-layered-MoS₂ nanosheets/graphene hybrid on cellulose paper for superior adsorption of methylene blue dye. *New J. Chem* 44, 5489–5500.
- Heibati, B., Rodriguez-Couto, S., Al-Ghouti, M.A., Asif, M., Tyagi, I., Agarwal, S., Gupta, V.K., 2015. Kinetics and thermodynamics of enhanced adsorption of the dye AR 18 using activated carbons prepared from walnut and poplar woods. *J. Mol. Liq.* 208, 99–105.
- Islam, M.A., Sabar, S., Benhouria, A., Khanday, W.A., Asif, M., Hameed, B.H., 2017. Nanoporous activated carbon prepared from karanj (*Pongamia pinnata*) fruit hulls for methylene blue adsorption. *J. Taiwan Inst. Chem. Eng.* 74, 96–104.
- Jawad, A.H., Abdulhameed, A.S., 2020. Statistical modeling of methylene blue dye adsorption by high surface area mesoporous activated carbon from bamboo chip using KOH-assisted thermal activation. *Energy Ecol. Environ.* 5 (6), 456–469.
- Jawad, A.H., Abdulhameed, A.S., Wilson, L.D., Syed-Hassan, S.S.A., Alothman, Z.A., Khan, M.R., 2021. High surface area and mesoporous activated carbon from KOH-activated dragon fruit peels for methylene blue dye adsorption: Optimization and mechanism study. *Chin. J. Chem. Eng.* 32, 281–290.
- Kazak, O., Eker, Y.R., Bingol, H., Tor, A., 2017. Novel preparation of activated carbon by cold oxygen plasma treatment combined with pyrolysis. *Chem. Eng. J.* 325, 564–575.
- Lacerda, V.S., López-Sotelo, J., Correa-Guimaraes, A., Hernández-Navarro, S., Sánchez-Báscones, M., Navas-Gracia, L.M., Martín-Ramos, P., Martín-Gil, J., 2015. Rhodamine B removal with activated carbons obtained from lignocellulosic waste. *J. Environ. Manage.* 155, 67–76.
- Li, Z., Hanafy, H., Zhang, L., Sellaoui, L., Netto, M.S., Oliveira, M.L.S., Selim, M.K., Dotto, G.L., Bonilla-Petriciolet, A., Li, Q., 2020a. Adsorption of congo red and methylene blue dyes on an ashitaba waste and a walnut shell -based activated carbon from aqueous solutions: Experiments, characterization and physical interpretations. *Chem. Eng. J.* 388, 124263.
- Li, T., Song, H.L., Xu, H., Yang, X.L., Chen, Q.L., 2021a. Biological detoxification and decolorization enhancement of azo dye by introducing natural electron mediators in MFCs. *J. Hazard. Mater.* 416, 125864.
- Li, X., Wang, K., Wang, M., Zhang, W., Yao, J., Komarneni, S., 2020b. Sustainable electrochemical dyeing of indigo with Fe(II)-based complexes. *J. Clean. Prod.* 276, 123251.
- Li, L., Wu, M., Song, C., Liu, L., Gong, W., Ding, Y., Yao, J., 2021b. Efficient removal of cationic dyes via activated carbon with ultrahigh specific surface derived from vinasse wastes. *Bioresour. Technol.* 322, 124540.
- Luo, Q.P., Huang, L., Gao, X., Cheng, Y., Yao, B., Hu, Z., Wan, J., Xiao, X., Zhou, J., 2015. Activated carbon derived from melaleuca barks for outstanding high-rate supercapacitors. *Nanotechnology* 26 (30), 304004.
- Menya, E., Olupot, P.W., Storz, H., Lubwama, M., Kiros, Y., 2018. Production and performance of activated carbon from rice husks for removal of natural organic matter from water: A review. *Chem. Eng. Res. Des.*, 271–296.
- Pagalan, E., Sebron, M., Gomez, S., Salva, S.J., Ampusta, R., Macarayo, A.J., Joyno, C.Q., Ido, A.L., Arazo, R.O., 2020. Activated carbon from spent coffee grounds as an adsorbent for treatment of water contaminated by aniline yellow dye. *Ind. Crop. Prod.* 145, 111953.
- Paredes-Laverde, M., Salamanca, M., Diaz-Corrales, J.D., Florez, E., Silva-Agredo, J., Torres-Palma, R.A., 2021. Understanding the removal of an anionic dye in textile wastewaters by adsorption on ZnCl₂ activated carbons from rice and coffee husk wastes: A combined experimental and theoretical study. *J. Environ. Chem. Eng.* 9 (4), 105685.
- Postai, D.L., Demarchi, C.A., Zanatta, F., Cipriani Melo, D.C., Rodrigues, C.A., 2016. Adsorption of rhodamine B and methylene blue dyes using waste of seeds of *Aleurites Moluccana*, a low cost adsorbent. *Alex. Eng. J.* 55 (2), 1713–1723.
- Rakesh, K., Gupta, M., Dubey, P., Kharel, Z., Gu, Q.i., 2015. Biochar activated by oxygen plasma for supercapacitors. *J. Power Sources* 274, 1300–1305.
- Saygili, H., Guzel, F., 2016. High surface area mesoporous activated carbon from tomato processing solid waste by zinc chloride activation: process optimization, characterization and dyes adsorption. *J. Clean. Prod.* 113, 995–1004.
- Shabaan, O.A., Jahin, H.S., Mohamed, G.G., 2020. Removal of anionic and cationic dyes from wastewater by adsorption using multiwall carbon nanotubes. *Arab. J. Chem.* 13 (3), 4797–4810.
- Silva, M.C., Spessato, L., Silva, T.L., Lopes, G.K.P., Zanella, H.G., Yokoyama, J.T.C., Cazetta, A.L., Almeida, V.C., 2021. H₃PO₄-activated carbon fibers of high surface area from banana tree pseudo-stem fibers: Adsorption studies of methylene blue dye in batch and fixed bed systems. *J. Mol. Liq.* 324, 114771.
- Suganya, S., Kumar, P.S., Saravanan, A., Rajan, P.S., Ravikumar, C., 2017. Computation of adsorption parameters for the removal of dye from wastewater by microwave assisted sawdust: Theoretical and experimental analysis. *Environ. Toxicol. Pharmacol.* 50 (March), 45–57.
- Toledo, P.V.O., Bernardinelli, O.D., Sabadini, E., Petri, D.F.S., 2020. The states of water in tryptophan grafted hydroxypropyl methylcellulose hydrogels and their effect on the adsorption of methylene blue and rhodamine B. *Carbohydr. Polym.* 248, 116765.
- Uddin, M.J., Ampiauw, R.E., Lee, W., 2021. Adsorptive removal of dyes from wastewater using a metal-organic framework: A review. *Chemosphere* 284, 131314.
- Wan, S., Wu, J., Zhou, S., Wang, R., Gao, B., He, F., 2018. Enhanced lead and cadmium removal using biochar-supported hydrated manganese oxide (HMO) nanoparticles: Behavior and mechanism. *Sci. Total Environ.*, 1298–1306.
- Wang, S.F., Chen, X.Y., Fang, L.M., Gao, H.J., Han, M.J., Chen, X. P., Xia, Y.H., Lei, X., Yang, H., 2022b. Double heterojunction CQDs/CeO₂/BaFe₁₂O₁₉ magnetic separation photocatalysts: Construction, structural characterization, dye and POPs removal, and the interrelationships between magnetism and photocatalysis. *Nucl. Anal.* 1, 100026.
- Wang, S., Gao, H., Jin, Y., Chen, X., Wang, F., Yang, H., Fang, L., Chen, X., Tang, S., Li, D., 2022a. Defect engineering in novel broad-band gap hexaaluminate MA112O19 (M = Ca, Sr, Ba)-Based photocatalysts Boosts Near ultraviolet and visible light-driven photocatalytic performance. *Mater. Today Chem.* 24, 100942.
- Wang, Q., Lai, Z., Luo, C., Zhang, J., Cao, X., Liu, J., Mu, J., 2021a. Honeycomb-like activated carbon with microporous nanosheets structure prepared from waste biomass cork for highly efficient dye wastewater treatment. *J. Hazard. Mater.* 416, 125896.
- Wang, S.F., Li, M.Y., Gao, H.J., Yin, Z.J., Chen, C.L., Yang, H., Fang, L.M., Jagadeesha Angadi, V., Yi, Z., Li, D.F., 2023. Construction of CeO₂/YMnO₃ and CeO₂/MgAl₂O₄/YMnO₃ photocatalysts and adsorption of dyes and photocatalytic oxidation of antibiotics: Performance prediction, degradation pathway and mechanism insight. *Appl. Surf. Sci.* 608, 154977.
- Wang, Z., Shen, D., Shen, F., Wu, C., Gu, S., 2017. Kinetics, equilibrium and thermodynamics studies on biosorption of Rhodamine B from aqueous solution by earthworm manure derived biochar. *Int. Biodeterior. Biodegrad.* 120, 104–114.
- Wang, T., Tang, X., Zhang, S., Zheng, J., Zheng, H., Fang, L., 2020. Roles of functional microbial flocculant in dyeing wastewater treatment: Bridging and adsorption. *J. Hazard. Mater.* 384, 121506.
- Wang, P., Wang, P., Guo, Y., Rao, L., Yan, C., 2021b. Selective recovery of protonated dyes from dye wastewater by pH-responsive BCN material. *Chem. Eng. J.* 412, 128532.

- Wang, H., Xu, J., Liu, X., Sheng, L., 2021c. Preparation of straw activated carbon and its application in wastewater treatment: A review. *J. Clean. Prod.* 283, 124671.
- Xia, Y., Jin, Y., Qi, J., Chen, H., Chen, G., Tang, S., 2021. Preparation of biomass carbon material based on *Fomes fomentarius* via alkali activation and its application for the removal of brilliant green in wastewater. *Environ. Technol. Innov.* 23, 101659.
- Xiao, W., Garba, Z.N., Sun, S., Lawan, I., Yuan, Z., 2020. Preparation and evaluation of an effective activated carbon from white sugar for the adsorption of rhodamine B dye. *J. Clean. Prod.* 253, 119989.
- Xiao, W., Jiang, X., Liu, X., Zhou, W., Garba, Z.N., Lawan, I., Wang, L., Yuan, Z., 2021. Adsorption of organic dyes from wastewater by metal-doped porous carbon materials. *J. Clean. Prod.* 284, 124773.
- Xue, S., Tu, B., Li, Z., Ma, X., Tao, H., 2021. Enhanced adsorption of Rhodamine B over *Zoysia sinica* Hance-based carbon activated by ammonium chloride and sodium hydroxide treatments. *Colloids Surf. A Physicochem. Eng. Asp.* 618, 126489.
- Zhang, J., Cui, F., Xu, L., Ma, Q., Gao, Y., Liu, Y., Cui, T., 2020a. Construction of magnetic NiO/C nanosheets derived from coordination polymers for extraordinary adsorption of dyes. *J. Colloid Interface Sci.* 561, 542–550.
- Zhang, Z., Xu, L., Liu, Y., Feng, R., Zhou, P., 2021. Efficient removal of methylene blue using the mesoporous activated carbon obtained from mangosteen peel wastes: Kinetic, equilibrium, and thermodynamic studies. *Microporous Mesoporous Mater.* 315, 110904.
- Zhang, Y., Yin, M., Sun, X., Zhao, J., 2020b. Implication for adsorption and degradation of dyes by Humic acid: light driven of Environmentally persistent free radicals to activate reactive oxygen species. *Bioresour. Technol.* 307, 123183.